Carbonate mineral paragenesis and reaction kinetics in the system MgO-CaO-CO$_2$-H$_2$O in presence of chloride or nitrate ions at near surface ambient temperatures.

Petra Kristova[a*], Laurence J. Hopkinson[b], Ken J. Rutt[a], Hazel M.A. Hunter[c,d] and Gordon Cressey[c]

[a] ([*]corresponding author) School of Pharmacy and Biomolecular Sciences,

University of Brighton.

Huxley Building, Lewes Road, Brighton.BN2 4GJ.

United Kingdom.

Tel: +44 (0)1273 642065, Fax: +44 (0)1273 642285, e.mail: p.kristova@brighton.ac.uk

Tel: +44 (0)1273 642076, Fax: +44 (0)1273 642285, e.mail: k.j.rutt@brighton.ac.uk

[b] School of the Environment and Technology,

University of Brighton

Cockcroft Building, Lewes Road, Brighton.BN2 4GJ.

United Kingdom.

Tel: +44 (0)1273 642239, Fax: +44 (0)1273 642285, e.mail: l.hopkinson@brighton.ac.uk

[c] Department of Mineralogy, Natural History Museum,

Cromwell Road, London, SW7 5BD,

United Kingdom.

Tel: +44 (0)20 7942 5711, Fax: +44 (0)20 7942 5537. e-mail: g.cressey@nhm.ac.uk

[d] ISIS Facility, STFC Rutherford Appleton Laboratory,

Harwell Oxford, Didcot, OX11 0QX,

United Kingdom.

Tel: +44 (0)1235 445116, e-mail: hazel.hunter@stfc.ac.uk

Key words: reaction kinetics, chlorartinite, monohydrocalcite, nesquehonite, dypingite,

hydromagnesite, CO_2 sequestration

Abstract

The reaction kinetics and solid phase products following the dissolution of $Mg(OH)_2$ by CO_2 sparging in the presence of calcium salts at 35°C, over a thirty day period have been studied. Experiments [A] and [B] were conducted with $CaCl_2$ salts with $[Mg^{2+}_{(aq)}:Ca^{2+}_{(aq)}]$ molar ratios 5:1 and 10:1 respectively. Experiment [S] employed $[Mg^{2+}_{(aq)}:Ca^{2+}_{(aq)} = 5:1]$ ratio but was seeded with hydromagnesite. Experiment [N] employed calcium nitrate $[Mg^{2+}_{(aq)}:Ca^{2+}_{(aq)} = 5:1]$. Results from all experiments show that magnesian calcite is the initial anhydrous carbonate to form, but with time this reacts and is replaced by aragonite formation. Towards the end of experiments formation of calcite/magnesian calcite is mildly increasing at the expense of aragonite. Aragonite production is coeval with the generation and progressive decomposition of nesquehonite $[Mg(HCO_3,OH)\cdot 2H_2O]$ forming $Mg_5(CO_3)_4(OH)_2\cdot xH_2O$ mineral phases (where $x = 8$ and 5 H_2O) in conjunction with subordinate barringtonite $[MgCO_3\cdot 2H_2O]$. The latter mineral is interpreted as an indicator of incongruent dissolution of nesquehonite. Experiments [A] and [B] document a short lived episode of chlorartinite $[Mg_2(CO_3)Cl(OH)\cdot 3H_2O]$ production, interpreted as an unstable intermediate between $Mg(OH)_2$ and $Mg(HCO_3,OH)\cdot 2H_2O$. Chlorartinite is not detected in experiment [S] indicating that either accelerated reaction rates in the seeded environment make the phase extremely short lived, or the direct path from $[Mg(OH)_2]$ to nesquehonite is kinetically favoured. Seeding also stimulated hydromagnesite growth. However it was insufficient to adequately ease supersaturation resulting in coeval nesquehonite formation and transformation. Aragonite formation in experiment [N] was delayed relative to the other experiments. This time delay suggests that until nitrate depletion was achieved through nitro-magnesium carbonate $[Mg(NO_3)_2\cdot 6H_2O]$ formation, precipitation of aragonite is suppressed. Based on all the experimental data, it is suggested that carbonate mineral paragenesis is driven by geochemical

feedback between a range of calcium and magnesium carbonate dissolution-precipitation events and is a sensitive function of the experimental conditions.

1. Introduction

Investigation of the CaO-MgO-CO$_2$-H$_2$O system at ambient temperatures is important for a greater understanding of mineral paragenesis in near surface conditions and is also a necessary precursor to the aim of storing carbon dioxide in carbonate mineral assemblages (e.g., Cipolli et al., 2004; Orlando et al., 2012; Ballirano et al., 2013). Magnesite [MgCO$_3$] and dolomite [CaMg(CO$_3$)$_2$] are the most stable magnesium-bearing carbonates under Earth surface conditions. However, it is well documented that in near surface settings carbonate mineral assemblages do not conform to those predicted by equilibrium thermodynamics (e.g., Kazakov et al., 1959; Davies and Bubela 1973; Morse and Casey 1988). Instead, a variety of partially characterized temperature sensitive basic and hydrated magnesium carbonates exist, which in at least some experimental settings appear to be the product of parallel reaction pathways (e.g., Hopkinson et al., 2012). In association with these phases other studies show that the presence of magnesium in solution may suppress calcite formation, facilitate aragonite precipitation (e.g., Park et al., 2008; Hu et al., 2009), lead to huntite [Mg$_3$Ca(CO$_3$)$_4$] and/or magnesian calcite formation (e.g., Bishoff 1985; Hopkinson et al., 2008), or give rise to other unstable species such as monohydrocalcite [CaCO$_3$·H$_2$O] (Nishiyama et al., 2013). Hence comparatively little is known of the parameters that control the nature of the relationships between calcium and magnesium metastable reaction products, although it seems likely that variation in the [Mg$^{2+}_{(aq)}$: Ca$^{2+}_{(aq)}$] ratio and seeding solutions with carbonate minerals are two parameters likely to exert strong control on mineral paragenesis.

In laboratory experiments calcium and magnesium carbonate minerals are generally synthesised by either mixing solutions of the relevant salt(s) with a solution containing a carbonate or bicarbonate salt (e.g., Hales et al., 2008) or by sparging CO$_2$ gas through solutions

of various salts. The latter method is often accompanied by CO_2 degassing induced by either increasing temperature and/or sonication (e.g. Hopkinson et al., 2012). Various combinations of the methods described above also exist including pH adjustments of the solutions (e.g., Ferrini et al., 2009; Ballirano et al., 2010). Salts commonly employed include chloride, nitrate and hydroxides. Although there does not seem to be any preference for specific starting materials other than in the investigation of magnesium chloride in relation to the sequestration of CO_2 in carbonate mineral phases in saline waters (De Vito et al., 2012). Hence the very nature of the synthesis method may have a bearing on reaction pathways. To these ends this study examines carbonate mineral paragenesis by CO_2 sparging and the progress of reaction pathways as a function of time and as a function of the $[Mg^{2+}_{(aq)}: Ca^{2+}_{(aq)}]$ ratio, aqueous solution seeding with hydromagnesite and, the comparative effect of employing chloride and nitrate salts on mineral paragenesis.

2. Methodology

The general experimental procedure involved dispersing powdered $Mg(OH)_2$ (Fluka Analytical, lot. 1442098V) and $CaCl_2.2H_2O$ (Fisher Scientific, lot. 1144526) or calcium nitrate (BDH, lot. 5789920B) in deionized water (300ml), stirring for 5 minutes and sparging with CO_2 at 150ml/minute for 4 hours at 25°C. The pH values were measured intermittently using a Mettler Toledo, MP220 pH meter (±0.01 pH) calibrated against pH 10 (borate), pH 7 (phosphate) and pH 4 (phthalate) NIST-traceable buffers (Fisher Scientific). All starting suspensions had an initial pH *ca.* 10.3. Subsequent to CO_2 sparging the pH stabilised at pH 7. Slurries were then transferred into a shaking water bath, speed 100rpm (VWR, Clifton) and held at 35°C for up to 30 days. Slurries were covered with pierced parafilm to avoid evaporation

and to allow exchange of gasses. Temperature was measured with a Fisher Scientific platinum sensor (Pt-100Ω) thermometer (± 0.1°C).

Experiments [A] and [B] employed [$Mg^{2+}_{(aq)}$:$Ca^{2+}_{(aq)}$] ratios of 5:1 and 10:1 respectively. Reaction [S] employed the same [$Mg^{2+}_{(aq)}$:$Ca^{2+}_{(aq)}$] ratio as [A] but was seeded with 0.002 mol of heavy hydromagnesite [$Mg_5(CO_3)_4(OH)_2 \cdot 5H_2O$] (Fisher Scientific, lot. 1164012) in place of 0.01 mol of $Mg(OH)_2$. Experiment [N] employed the same protocol as experiment [A] but with calcium chloride replaced by a molar equivalent of calcium nitrate (Table 1). For each experimental set, nine initial preparations were started; each of these nine reactions were arrested sequentially after increasingly longer periods of time, in order to characterize the solid phases and their amounts produced as a function of time. Precipitates recovered by vacuum filtration were dried at room temperature for 48 hours without washing, in an effort to maintain representative concentrations of any high solubility mineral phases. Dried samples were lightly ground in an agate mortar prior to analyses. Samples are coded with a letter denoting experiment type and a number indicating experimental duration (in days). Zero days duration refers to samples collected immediately after sparging.

Reaction name	Magnesium salt(s)	Calcium salt	Ratio of Mg:Ca
A	0.1 mol (5.83grams) magnesium hydroxide [$Mg(OH)_2$]	0.02 mol (2.94 grams) calcium chloride [$CaCl_2.2H_2O$]	5:1
B	0.1 mol (5.83grams) magnesium hydroxide [$Mg(OH)_2$]	0.01mol (1.47 grams) calcium chloride as [$CaCl_2.2H_2O$]	10:1
S	0.09 mol (5.22grams) magnesium hydroxide [$Mg(OH)_2$] and 0.002 mol (0.93 grams) magnesium carbonate heavy [$Mg_5(CO_3)_4(OH)_2.xH_2O$]	0.02 mol (2.94 grams) calcium chloride [$CaCl_2.2H_2O$]	5:1
N	0.1 mol (5.83grams) magnesium hydroxide [$Mg(OH)_2$]	0.02 mol calcium nitrate [$Ca(NO_3)_2$] (3.30 grams)	5:1

Table 1: Summary of reactants used in experiments.

Precipitates were characterized by Raman and mid-infrared spectroscopy, both conducted at the University of Brighton (U.K.). X-ray powder diffraction (XRD) was performed at the Natural History Museum, London (U.K.). All analyses were conducted at 25°C and at atmospheric pressure. Raman analyses were conducted using a Perkin Elmer Raman Identicheck fitted with a 785nm laser, a CCD detector and a fiber optic probe with 70mW laser power. The fiber optic probe has a spot size 100μm spot size at a working distance of 7.5mm. The samples were measured in the spectral range 2000-150cm^{-1} at resolution of 2cm^{-1}. Each spectrum was collected from 8 scans for 2 seconds and repeated six times on different randomly selected subsamples to assure representative spectral information. The Raman spectra obtained were averaged and baseline corrected; the limit of detection is *ca.* 2% or better (Kristova et al., 2013). Data manipulation was performed using the software Spectrum (Perkin Elmer) and PeakFit (Jandel, Scientific Software). Mid-infrared spectroscopic measurements were collected on a Perkin Elmer Spectrum 65 spectrometer fitted with an attenuated total reflection accessory. The samples were measured in the spectral range 4000-600cm^{-1} at a resolution of 4cm^{-1}. Each spectrum was collected from 16 scans at 25°C.

X-ray powder diffraction (XRD) data were collected using a Nonius PDS120 Powder Diffraction System with an INEL curved position sensitive detector. This detector has an output array of 4096 digital channels representing an arc of 120°2θ and permits the simultaneous measurement of diffracted X-ray intensities at all angles of 2θ across 120° with a static beam-sample-detector geometry. Copper (or, in a parallel set of experiments, Cobalt) Kα$_1$ radiation was selected from the line focus of the primary beam using a germanium 111 single-crystal monochromator and a post-monochromator horizontal slit. Horizontal and vertical slits were

used to restrict the beam to 0.24 by 5.0mm (or, for Co radiation, 0.14 by 5.0mm) respectively. Thin-smear powdered samples were mounted on a single-crystal quartz substrate, and measurements made in reflection geometry with the sample surface (spinning in its own plane) at an angle of ~2° to the incident beam. Data collection times were 30 minutes for each sample. NIST Silicon powder SRM640 and silver behenate were used as external 2θ calibration standards and the 2θ linearization of the detector was performed using a least-squares cubic spline function. Mineral phase identification was undertaken by search-match procedures using the PDF-2 database supplied by the International Centre for Diffraction Data (ICDD). The detection limit for mineral phase(s) in mixed assemblages of basic and hydrate magnesium carbonates is *ca* 5% modal abundance.

3. Results

Figure 1 summarises the variation of pH and v_1 Raman intensity for the major common phases nesquehonite, dypingite-type [$Mg_5(CO_3)_4(OH)_2 \cdot xH_2O$] and calcium carbonates for each experiment plotted against reaction time. The relative abundance of $CaCO_3$ polymorphs was constrained as the ratio of vaterite (v_4 753cm^{-1}) to calcite (v_4 713cm^{-1}) to aragonite (lattice mode 208cm^{-1}) by peak height. Figure 2 illustrates the typical FT-IR and Raman spectra obtained. Mid-infrared data indicates evidence of (OH) groups in samples devoid of evidence for $Mg_5(CO_3)_4(OH)_2 \cdot xH_2O$ suggesting that $Mg(HCO_3,OH) \cdot 2H_2O$ is present in abundance relative to, or possibly to the exclusion of, $Mg(CO_3) \cdot 3H_2O$ in those samples analyzed. A representative IR spectrum is shown in Figure 2a, together with examples of curve-fitted Raman spectra in the carbonate v_1 region from four selected samples (Figure 2b-e). The following section examines these plots in detail, for each experimental time series, with mineral identification confirmed by XRD.
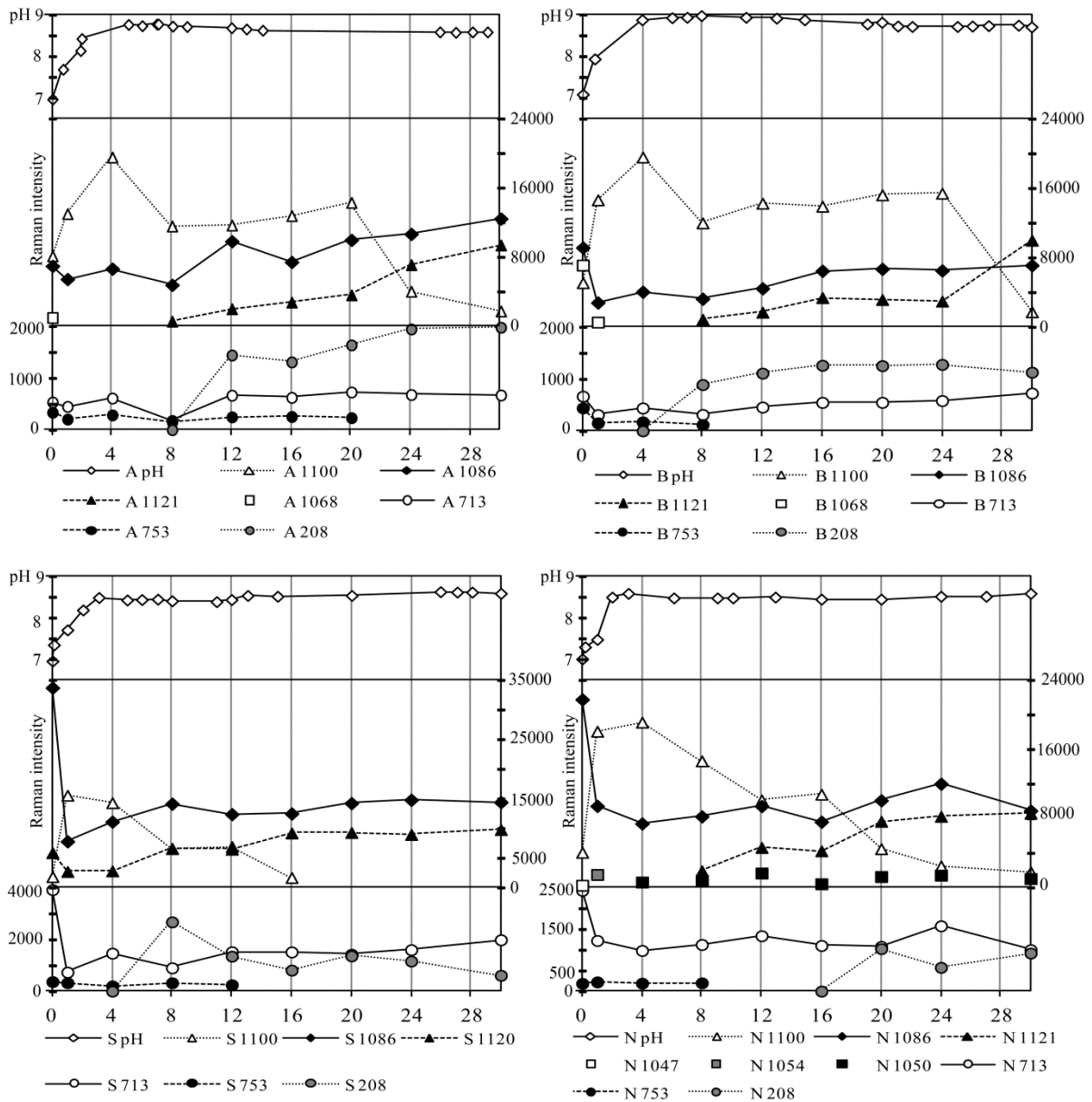
Figure 1: Experimental results plotted against time (in days) for: a) Experiment [A], b) Experiment [B], c) Experiment [S], d) Experiment [N] where each shows pH measurements (top), Raman semi-quantitative measurements of ν_1 peaks for main mineral phases plotted in absolute values (middle) and Raman semi-quantitative measurements of calcium carbonate phases in absolute values (bottom).
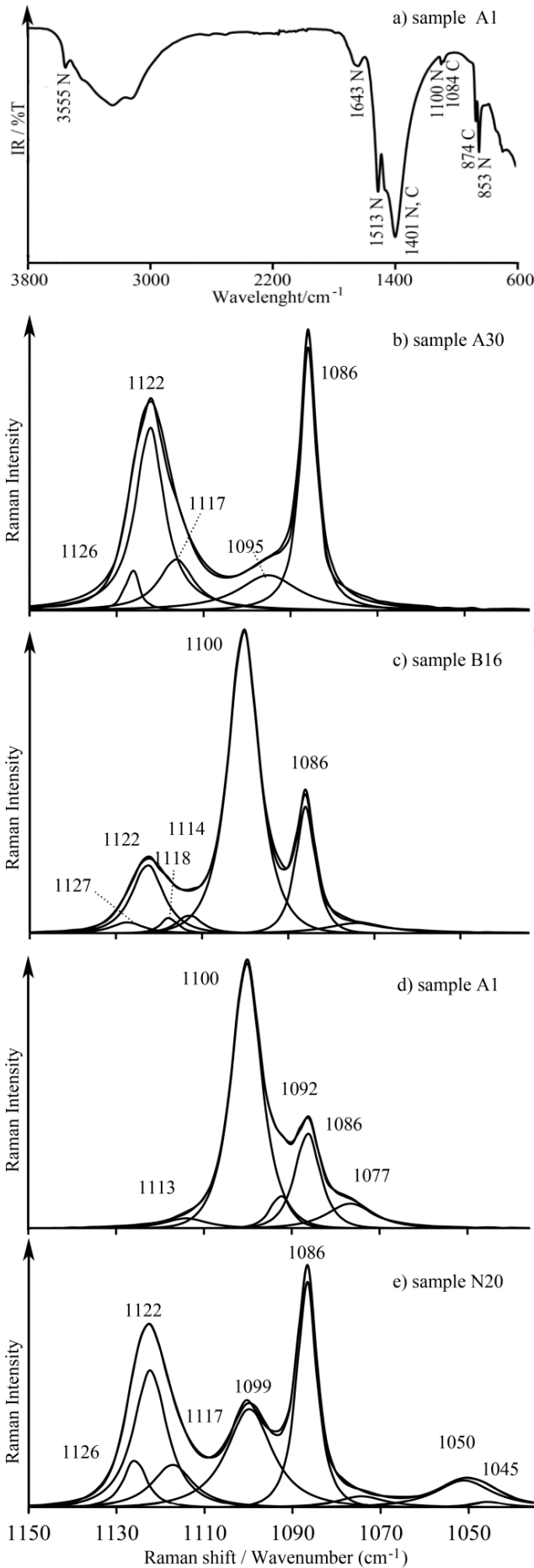
Figure 2: Representative (a) FT-IR and (b-e) Raman spectra showing detail of curve fitting in the range 1150-1030cm^{-1}. a) FT-IR spectrum of A1 sample containing nesquehonite with OH band at 3555cm^{-1}. N denotes nesquehonite, C denotes calcium carbonate. Vaterite could not be distinguished by IR due to its low concentration and spectral overlap with calcite peaks. Raman spectra for samples b) A30, c) B16, d) A1 and e) N20.

3.1 Experiment [A]

Raman and XRD show that Mg-calcite (v_I 1088cm^{-1}) with subordinate vaterite (v_I 1077cm^{-1}) were the dominant [CaCO$_3$] polymorphs until (A12), and thereafter aragonite is the main CaCO$_3$ phase produced (Figure 1a). Sample (A0) shows a shoulder on the (v_I 1088cm^{-1}) internal mode at 1069cm^{-1} consistent with short lived traces of CaCO$_3$·H$_2$O in the system. Evidence for traces of vaterite persists until (A20).

The v_1 band of nesquehonite [MgCO$_3$·3H$_2$O] or [Mg(HCO$_3$,OH)·2H$_2$0] situated at 1100cm^{-1} attains maximum intensity in (A4), decreasing and then stabilizing (or marginally increasing) in intensity (A8 - A20) and thereafter rapidly diminishing in intensity (Figure 1). From (A8) onwards a band at 1122cm^{-1} appears and progressively grows in intensity with increasing experimental duration. The band is assigned to dypingite-type [Mg$_5$(CO$_3$)$_4$(OH)$_2$·xH$_2$O] phase(s). XRD identified that dypingite [Mg$_5$(CO$_3$)$_4$(OH)$_2$.8H$_2$O] forms first (A4 - A8) with both forms [Mg$_5$(CO$_3$)$_4$(OH)$_2$.8H$_2$O] and [Mg$_5$(CO$_3$)$_4$(OH)$_2$.5H$_2$O] present thereafter.

Analysis of the broad spectral feature at *ca* 1122cm^{-1} with a Gaussian Lorentzian function suggests that it consists of four overlapping peaks: the most intense at 1122cm^{-1}, two weak peaks at 1117cm^{-1} and 1126cm^{-1}, all of which increase in intensity with increasing experimental duration, plus a poorly resolved very weak band at *ca* 1114cm^{-1}.

The position of the high intensity band at 1122cm^{-1} closely coincides with the reported v_1 [CO$_3$$^{2-}$] internal mode for dypingite *ca* 1120cm^{-1} (Frost et al., 2009). The origins of the 1117cm^{-1} and 1126-1127cm^{-1} bands are uncertain and do not serve to discriminate the eight from five waters of crystallization in Mg$_5$(CO$_3$)$_4$(OH)$_2$·xH$_2$O   phases. Previous studies have shown that

$Mg_5(CO_3)_4(OH)_2 \cdot xH_2O$ phases show distinct unit cell parameters yet retain essentially uniform short-range order of the CO_3^{2-} anion (Hopkinson et al., 2012). However, studies also indicate that dypingites have variable structural H_2O content and their CO_3^{2-} units are variably distorted (Frost et al., 2009). Further, the $1117cm^{-1}$ band closely coincides with the reported v_1 vibration of hydromagnesite at $1116\text{-}1119cm^{-1}$ (e.g., Edwards et al., 2005; Martinez-Arkanzo et al., 2007) whilst doubling of v_1 components in the range $1110cm^{-1}$ and $1120cm^{-1}$ has been assigned to distinct CO_3^{2-} ions in the structure of hydromagnesite (White 1974). Hence, it is possible that doubling of v_1 components in the $Mg_5(CO_3)_4(OH)_2 \cdot xH_2O$ phases reported here extends to higher frequencies than that reported for hydromagnesite. XRD analysis indicates the presence of small quantities of chlorartinite $[Mg_2(CO_3)Cl(OH) \cdot 3H_2O]$ in (A0) through to (A24) (Figure 3). Raman identification of the mineral phase is complicated by the closely spaced overlapping spectral features in the $1122cm^{-1}$ region. However, the main Raman active v_1 internal mode for chlorartinite is reported at $1114cm^{-1}$ (RRUFF database). Hence, the very low intensity feature at $1114cm^{-1}$ resolved by peak fit software is assigned to chlorartinite.
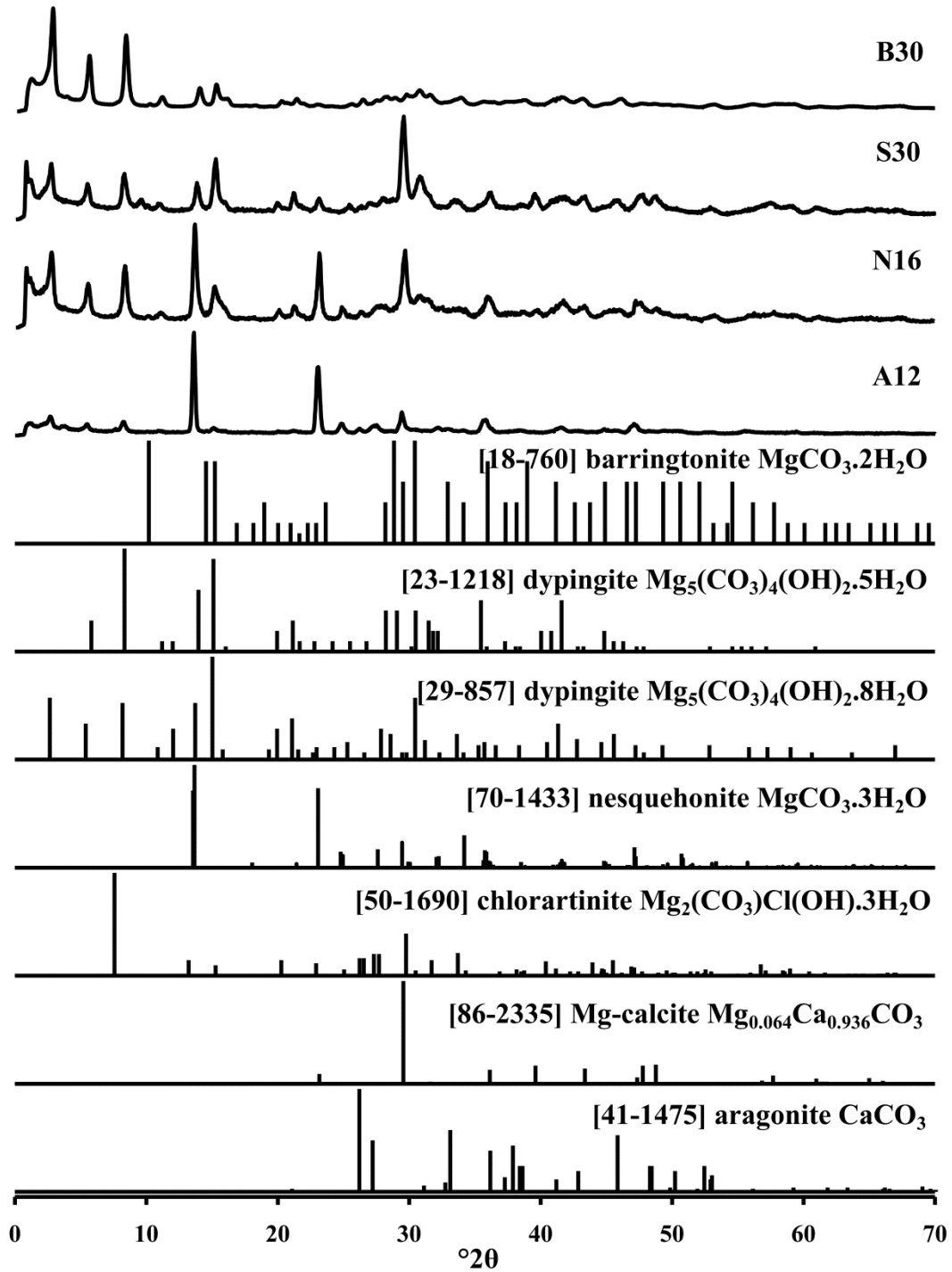
Figure 3: X-ray diffraction pattern of samples: a) B30, b) S30, c) N16, d) A12, with relevant theoretical patterns shown for reference.

After 30 days reaction the (A30) diffraction pattern indicates that traces of barringtonite [$MgCO_3 \cdot 2H_2O$] may also be present (d=8.75Å, Cu=10.1°2Θ, Co=11.7°2Θ), a phase for which no Raman spectrum exists. However, the Raman spectra reported here do show a low intensity feature at *ca* 1094-1095cm^{-1}. Several carbonate minerals show a strong Raman peak in this area e.g. magnesite, artinite, vaterite and an unnamed hydrous Ca-bearing magnesium carbonate (HCMC) (Queralt et al., 1997; Edwards et al., 2005). However, none of them were identified by XRD. Hence available evidence suggests that barringtonite, or a barringtonite-like magnesium hydrate carbonate, is characterized by a high intensity band at 1094-1095cm^{-1} and is associated with the decomposition of nesquehonite alongside the generation of volumetrically abundant $Mg_5(CO_3)_4(OH)_2 \cdot xH_2O$ phases.

3.2 Experiment [B]

Sample (B0) shows a predominant peak at 1087cm^{-1} assigned to $CaCO_3$ polymorphs, a subordinate peak at 1068cm^{-1} assigned to monohydrocalcite [$CaCO_3 \cdot H_2O$] and a low intensity peak at 1100cm^{-1} assigned to nesquehonite (Figure 1b). XRD and Raman indicate that aragonite is the dominant $CaCO_3$ polymorph although calcite/magnesian calcite grows from day 8 onwards. XRD indicates that traces of chlorartinite [$Mg_2(CO_3)Cl(OH) \cdot 3H_2O$] are present in samples (B0) through to (B20). In common with experiment [A] the 1100cm^{-1} peak (assigned to nesquehonite) attains its maximum intensity in sample (B4) and then diminishes, coincident with emergence of $Mg_5(CO_3)_4(OH)_2 \cdot xH_2O$ phase(s). In the (B8-B30) time frame XRD indicates that $Mg_5(CO_3)_4(OH)_2 \cdot 8H_2O$ forms first, and is later accompanied by $Mg_5(CO_3)_4(OH)_2 \cdot 5H_2O$. Again analysis of the broad spectral feature at *ca* 1122cm^{-1} using a Gaussian Lorentzian function shows that the feature consists of four overlapping peaks: 1122cm^{-1} (highest intensity) followed by 1117cm^{-1}, 1126cm^{-1} and a very weak band at 1114cm^{-1} (assigned to chlorartinite).

Both XRD and Raman also show evidence for $MgCO_3 \cdot 2H_2O$ in the final stages of the experiment (Figure 3). These results differ from experiment [A] in three respects. Namely, the abrupt reduction in nesquehonite content towards the end of the experiment commences four days later than in experiment [A], vaterite is not resolved beyond (B8) (compared to (A20)) and monohydrocalcite $[CaCO_3 \cdot H_2O]$ is identified in the (B1) sample indicating that it can persist beyond the sparging stage in the experiment [B] regime. Monohydrocalcite is metastable with respect to calcite and aragonite (e.g., Taylor 1975; Kamiya et al., 1977; Munemoto and Fukushi 2008) and readily transforms into either $CaCO_3$ polymorph (Kamiya et al., 1977; Loste et al., 2003).

3.3 Experiment [S]

Solids collected after sparging (S0) consisted of calcite (v_1 1088cm^{-1}), seeded hydromagnesite (v_1 1119cm^{-1}) and traces of vaterite (v_4 753cm^{-1}) (Figure 1c). Aragonite appears after four days, peaks in concentration in (S8) and thereafter its presence gradually decreases. Vaterite is lost from the system after (S12), whereas calcite (v_4 713cm^{-1}) marginally increases in concentration throughout. XRD showed that all samples contain hydromagnesite $[Mg_5(CO_3)_4(OH)_2 \cdot 4H_2O]$, however, (S0) contains the least amount. Nesquehonite appears in (S1) and attains a maximum concentration in (S4); it is not resolved beyond (S16). Peak fitting of the Raman spectrum of (S4) in the carbonate v_1 region indicates that nesquehonite formation is followed by the emergence of a weak band at 1125cm^{-1}, consistent with traces of $Mg_5(CO_3)_4(OH)_2 \cdot xH_2O$ phases. With increasing experimental duration this peak attains parity in intensity (S8-S12) with the v_1 internal mode of nesquehonite, while the hydromagnesite v_1 peak shifts to 1120cm^{-1}. Between (S16 - S30) the multicomponent $Mg_5(CO_3)_4(OH)_2 \cdot xH_2O$ peak in the v_1 region shows

maximum intensity. XRD shows close agreement with Raman findings and indicates traces of barringtonite or a barringtonite-like phase develop at the end of the experiment (S30).

3.4 Experiment [N]

Calcite is the dominant $CaCO_3$ polymorph from the outset with aragonite forming between (N16–N30) and traces of a vaterite-like phase present until (N8) (Figure 1d). Nesquehonite precipitation occurs in (N1–N4) with later concentrations diminishing, to trace levels by (N30), coincident with a progressive rise in $Mg_5(CO_3)_4(OH)_2 \cdot xH_2O$ content. Specific to experiment [N] is the appearance of Raman active bands at $1047 cm^{-1}$, $1054 cm^{-1}$ and $1050 cm^{-1}$ (Figure 2e). The precise origins of these bands are uncertain although nitrocalcite [$Ca(NO_3)_2 \cdot 4H_2O$)] and nitromagnesite [$Mg(NO_3)_2 \cdot 6H_2O$] have previously been reported with high intensity peaks at $1048 cm^{-1}$ and $1058 cm^{-1}$ respectively (Martinez-Arkarazo et al., 2007). Similar Raman bands have also been observed for nitrate adsorption on hydroxide compounds (hydrotalcite) and were assigned to the non-hydrogen bonded, and to the hydrogen bonded, symmetrical stretch of NO_3^- at $1045 cm^{-1}$ and $1050 cm^{-1}$ respectively (Frost et al., 2005; Frost and Musumeci 2006). Hence, the Raman bands identified in experiment [N] are assigned to nitrate related compounds. XRD detected the presence of magnesium nitrate hexahydrate [$Mg(NO_3)_2 \cdot 6H_2O$] in samples (N16) onwards (Figure 3). This may suggest that nitrate-assigned Raman active bands in samples prior to day 16 are contained within the product phases either as dispersed inclusions, between structural layers, and/or as a discrete X-ray amorphous phase(s). In common to all experiments sample (N30) shows a low intensity peak at *ca* $1095 cm^{-1}$ which is progressively resolved as the concentration of nesquehonite diminishes. This band is tentatively assigned to barringtonite [$MgCO_3 \cdot 2H_2O$].

4. Discussion

4.1 Presence of chlorartinite.

Traces of chlorartinite [$Mg_2(CO_3)Cl(OH)\cdot3H_2O$] were detected by XRD in samples from experiments [A] and [B] over the first 20 days, only. The mineral phase initially occurs in association with $Mg(OH)_2$ and $Mg(HCO_3,OH)\cdot2H_2O$, indicating that its formation preceded, at least in part, nesquehonite decomposition and the coeval generation of $Mg_5(CO_3)_4(OH)_2\cdot xH_2O$ phases. Chlorartinite and artinite have not been reported as metastable intermediates of the nesquehonite to hydromagnesite transition (e.g., Davies and Bubela 1973). Although little is known about the stability field of chlorartinite, low temperature thermodynamic models indicate that the closely related mineral artinite [$Mg_2(CO_3)(OH)_2\cdot3H_2O$] occupies a pCO_2 stability field between brucite and nesquehonite (Könisberger et al., 1999) and has been reported with between two to four water molecules (e.g., Beck 1950; Kazakov et al., 1959). More recent experiments involving sparging CO_2 through $MgCl_2\cdot6H_2O$ aqueous solutions have demonstrated that chlorartinite formation was followed by abundant nesquehonite precipitation (Mignardi et al., 2011; De Vito et al., 2012). This suggests that chlorartinite is likely to be the first carbonate phase formed in our system, accompanying $Mg(OH)_2$ dissolution.

The transition from chlorartinite and artinite to nesquehonite is only partially documented (Kazakov et al., 1959; De Vito et al., 2012). However, in MgO-H_2O-CO_2 space chlorartinite falls on a line that connects brucite [$Mg(OH)_2$] with nesquehonite (Figure 4). No protohydromagnesite [$Mg_5(CO_3)_4(OH)_2\cdot11H_2O$] was identified in the experiments documented here, which may suggest that the direct reaction path to nesquehonite was kinetically favoured over the indirect path *via* protohydromagnesite. The apparent absence of chlorartinite in experiment [S] may suggest that accelerated reaction rates in the seeded environment either

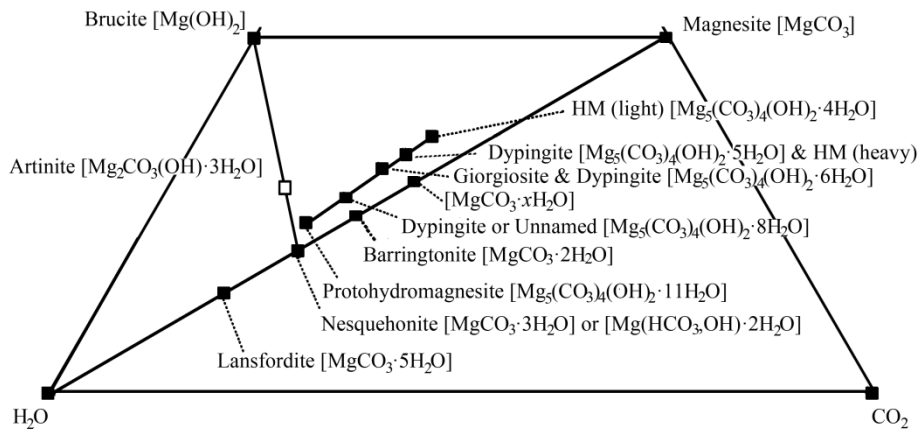make the phase extremely short lived, or the direct path from $Mg(OH)_2$ to nesquehonite is kinetically favoured.

Figure 4: The hydrated magnesium carbonate minerals in the system CO_2-MgO-H_2O, adapted from Canterford et al., (1984) and Hopkinson et al., (2012). A pathway is suggested between brucite, artinite and nesquehonite; see Hopkinson et al., (2012) for further details of mineral names. The unnamed mineral $[Mg_5(CO_3)_4(OH)_2 \cdot 8H_2O]$ is not listed by the International Mineralogical Association although it is listed as dypingite in the XRD database Powder Diffraction File PDF-2 supplied by the International Centre for Diffraction Data (ICDD). HM denotes hydromagnesite. Specified values of x in synthesised $MgCO_3 \cdot xH_2O$ phases include 1.3 and 0.3 H_2O (Zhang et al., 2006). The ternary plot is shown here without its MgO apex.

4.2 Hydromagnesite seeding.

Experimental results show that seeding the mother liquor with hydromagnesite effectively halved the time it takes for nesquehonite to disappear from the system, relative to experiments [A] and [B]. Seeding also stimulates post-sparging hydromagnesite growth. Previous studies (e.g., Königsberger et al., 1999; Hopkinson et al., 2012) indicate that in all four experiments the system would have been simultaneously supersaturated with nesquehonite and hydromagnesite, yet formation of hydromagnesite is restricted to experiment [S]. Data also

indicates that formation of $Mg_5(CO_3)_4(OH)_2 \cdot xH_2O$ dypingite-type phases (for which no thermodynamic data exists) occurs at the expense of nesquehonite. Combined this suggests that nucleation of hydromagnesite on existing hydromagnesite seeds is inadequate to ease supersaturation, to the extent that crystallization becomes governed by the disorder of the system (e.g., Goldsmith 1953). Thereby nucleation and growth of nesquehonite occurs in conjunction with hydromagnesite growth.

4.3 Presence of barringtonite.

XRD indicates that traces of barringtonite [$MgCO_3 \cdot 2H_2O$] or a barringtonite-like magnesium carbonate hydrate is associated with the decomposition of nesquehonite alongside volumetrically abundant $Mg_5(CO_3)_4(OH)_2 \cdot xH_2O$ phases (with eight and five waters of crystallization) towards the end of all four experiments reported here. Some studies have shown that $MgCO_3 \cdot xH_2O$ phases (where $x \leq 3H_2O$) can be generated during the transformation of nesquehonite to hydromagnesite in an aqueous medium (e.g., Hopkinson et al., 2008). Conversely, other experiments show that the transformation of nesquehonite to hydromagnesite can occur in the absence of resolvable $MgCO_3 \cdot xH_2O$ phases (where $x \leq 3H_2O$). Instead, intermediate $Mg_5(CO_3)_4(OH)_2 \cdot xH_2O$ phases between nesquehonite and hydromagnesite have been reported, which show eleven (Davies and Bubela, 1973) or eight and five waters of crystallization (Hopkinson et al., 2012). It is firmly established that the water content in $MgCO_3 \cdot xH_2O$ phases are strongly affected by synthesis conditions, and that these phases may contain some bicarbonate (Zhang et al., 2006). Furthermore desiccation of nesquehonite yields $MgCO_3 \cdot H_2O$ (Menzel and Brückner 1930; Dell and Weller 1959) and although the congruency of nesquehonite dissolution is uncertain, it is possible that dissolution of nesquehonite at least

in some settings may involve preferential loss of waters of crystallization and/or breakdown of bicarbonate to yield barringtonite.

$$Mg(HCO_3,OH)\cdot 2H_2O \rightarrow MgCO_3\cdot 2H_2O + H_2O_{(aq)}$$
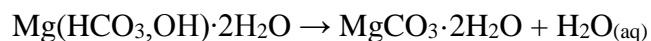
The potential significance of this proposed reaction, combined with the fact that conditions of synthesis affect the magnesium hydrate water content and the possibility that nesquehonite may undergo incongruent water loss, is that an alternative starting point may be thus generated prior to the parallel reaction pathway (in particular transformation of metastable $Mg_5(CO_3)_4(OH)_2\cdot xH_2O$ phases towards hydromagnesite [$Mg_5(CO_3)_4(OH)_2\cdot 4H_2O$]). Variations in the nature and appearance of the $Mg_5(CO_3)_4(OH)_2\cdot xH_2O$ phases will be governed by the precursor or evolving chemistry of the unstable magnesium hydrate species. This interpretation accounts for the apparent disparities in the numbers and types of mineral phases reported to arise from the nesquehonite to hydromagnesite transition. Accepting this, it also follows that the mineral protohydromagnesite [$Mg_5(CO_3)_4(OH)_2\cdot 11H_2O$] which shows the closest compositional similarity to nesquehonite, reported composition $MgCO_3\cdot 3H_2O$ (Davies and Bubela 1973), may represent the closest approach to congruent dissolution of nesquehonite and thereby the most extended possible parallel reaction pathway of $Mg_5(CO_3)_4(OH)_2\cdot xH_2O$ phases to hydromagnesite.

4.4 Behaviour of calcium carbonate phases.

Monohydrocalcite [$CaCO_3\cdot H_2O$] is restricted in occurrence to the opening period (*ca* 1 day) of experiment [B] in which the mineral occurs alongside magnesian calcite, lesser quantities of vaterite and progressively abundant nesquehonite. It has been observed (Nishiyama et al., 2013) that monohydrocalcite formation concurrent with nesquehonite requires the presence of

magnesium in solution and more CO_3^{2-} than $Ca^{2+}_{(aq)}$ because the high hydration energy of magnesium prevents quick $CaCO_3 \cdot H_2O$ dehydration to anhydrous calcium carbonate. Evidently these conditions were temporarily met during the onset of experiment [B]. In this respect our experimental results, which indicate that a magnesium to calcium ratio of 10 or more is required for $CaCO_3 \cdot H_2O$ formation, are in keeping with the previous findings of Nishiyama et al. (2013). The disappearance of monohydrocalcite is coincident with the widespread onset of nesquehonite precipitation, suggesting that the latter process is coincident with $CaCO_3 \cdot H_2O$ dehydration. It has been suggested that $CaCO_3 \cdot H_2O$ forms via the transformation of a calcium-rich hydrated magnesium-bearing amorphous carbonate precursor (Nishiyama et al., 2013), in which the transformation to monohydrocalcite occurs because dehydration is prevented by the presence of an external layer composed of hydrous Mg-carbonate. Accepting this, it follows that $CaCO_3 \cdot H_2O$ dehydration may have arisen because of the loss of hydrated Mg carbonate external groups from an amorphous carbonate precursor as a consequence of nesquehonite formation.

Experimental results show that the dominant anhydrous carbonate to form in the early stages of the experiments is magnesian calcite, with subordinate vaterite. Subsequently the dominant metastable polymorph is aragonite. Vaterite is commonly formed in experimental settings when $CaCO_3$ is rapidly precipitated (e.g., Hopkinson et al., 2008). The vaterite polymorph is unstable with respect to calcite and in an aqueous medium can rapidly transform to calcite through dissolution-precipitation reactions. The Mg^{2+} ion is known to accelerate this crystal transformation process (Chen et al., 2006).

Previous studies indicate that the presence of magnesium can retard or inhibit calcite crystallization and kinetically favor the formation of aragonite (e.g., Berner 1975; Reddy and

Wang 1980). However independent studies show that if the MgO-CaO-CO_2-H_2O system exists at high supersaturation then calcite precipitates first (Fernandez-Diaz et al., 1996; Hu and Deng 2004) thereby potentially accounting for the presence of magnesian calcite prior to the onset of aragonite formation in the experiments documented here. Another possible reason favoring magnesian calcite formation relative to aragonite during CO_2 sparging relates to the higher solubility of the calcium salts (chloride, nitrate) relative to $Mg(OH)_2$, which may have facilitated reaction between calcium ions and CO_2 earlier than reactions between magnesium and CO_2. Previous experimental studies have shown significant differences in reaction times between bicarbonate with calcium and magnesium ions (Bonales et al., 2013).

Aragonite formation relative to calcite is favored when the precipitation rate, and especially the supply rate of CO_3^{2-} ions, is high (Hu and Deng 2004). In the experiments documented here, aragonite mainly precipitated during nesquehonite dissolution which is consistent with aragonite formation in conditions of low supersaturation with respect to calcium with nesquehonite dissolution providing a supply of CO_3^{2-} and Mg^{2+} ions. Results also show that although nesquehonite is unstable with respect to dypingite there is some evidence for more than one wave of nesquehonite formation (Figure 1). This may be consistent with a scenario in which the rate of nesquehonite dissolution proceeds at a faster rate than dypingite formation, in the process generating excess bicarbonate which is then periodically consumed during the formation of aragonite and nesquehonite until the excess bicarbonate is depleted.

Employing nitrate salts in the synthesis programme had no marked effect on the crystal chemistry of nesquehonite nor the overall nature of magnesium carbonate paragenesis in comparison to experiment [A]. However, aragonite formation in experiment [N] occurs conspicuously later than in experiments [A], [B] or [S]. One possible explanation is that

aragonite precipitation was suppressed until nitrate depletion was achieved through nitro-magnesium carbonate [$Mg(NO_3)_2 \cdot 6H_2O$] generation.

5. Conclusions

Experiments [A] and [B] demonstrate that dissolution of $Mg(OH)_2$ by CO_2 sparging facilitated chlorartinite [$Mg_2(CO_3)Cl(OH) \cdot 3H_2O$] generation and abundant nesquehonite [$Mg(HCO_3,OH) \cdot 2H_2O$] formation. From this it is suggested that chlorartinite may represent a first formed intermediate between brucite [$Mg(OH)_2$] and nesquehonite. The absence of chlorartinite in a hydromagnesite-seeded environment suggests either that accelerated reaction rates made the phase extremely short lived, or that the direct path from $Mg(OH)_2$ to nesquehonite was kinetically favoured. Progressive decomposition of nesquehonite [$Mg(HCO_3OH) \cdot 2H_2O$] is accompanied by the generation of abundant $Mg_5(CO_3)_4(OH)_2 \cdot xH_2O$ mineral phases with subordinate barringtonite [$MgCO_3 \cdot 2H_2O$] detected after 30 days reaction. The latter mineral is interpreted to result from incongruent dissolution of nesquehonite. This further suggests that the length of the $Mg_5(CO_3)_4(OH)_2 \cdot xH_2O$ reaction pathway from nesquehonite to hydromagnesite may be a precise function of nesquehonite dissolution kinetics and/or conditions of synthesis, thereby accounting for the disparity in experimental results reported from independent investigations on the nesquehonite to hydromagnesite transition (e.g., Davies and Bubela 1973; Zhang et al., 2006; Hopkinson et al., 2008, 2012).

In agreement with previous studies, when the magnesium to calcium ratio exceeds 10 or more, as in experiment [B], monohydrocalcite [$CaCO_3 \cdot H_2O$] is produced. Loss of monohydrocalcite

from the system coincides with nesquehonite formation, and is consistent with geochemical feedback between Ca and Mg carbonates driving mineral paragenesis. Magnesian calcite formation followed by aragonite generation coincident with nesquehonite formation and its subsequent transformation to dypingite-type phases is common to the four experiments. This is consistent with aragonite formation being favored in conditions of low supersaturation with respect to calcium, with nesquehonite dissolution providing a supply rate of CO_3^{2-} and Mg^{2+} ions. The differing solubilities of the calcium salts relative to $Mg(OH)_2$ may also have significant bearing on the particular $CaCO_3$ polymorph that nucleates and grows. Formation of magnesium nitrate hexahydrate $[Mg(NO_3)_2 \cdot 6H_2O]$ is exclusive to experiment [N], the appearance of which exerts strong control on the timing of aragonite formation.

Acknowledgements

References

Ballirano, P., De Vito, C., Ferrini, V. and Mignardi, S. (2010) The thermal behaviour and structural stability of nesquehonite, $MgCO_3 \cdot 3H_2O$, evaluated by *in situ* laboratory parallel-beam X-ray powder diffraction: New constraints on CO_2 sequestration within minerals. *Journal of Hazardous Materials*, 178, 522–528.

Ballirano, P., De Vito, C., Mignardi, S. and Ferrini, V. (2013) Phase transitions in the Mg-CO_2-H_2O system and the thermal decomposition of dypingite, $Mg_5(CO_3)_4(OH)_2.5H_2O$: Implications for geosequestration of carbon dioxide. *Chemical Geology*, 340, 59-67.

Beck, C.W. (1950) Differential thermal analysis curves of carbonate minerals. *American Mineralogist,* 35, 985-1013.

Berner, R.A. (1975) The role of magnesium in the crystal growth of calcite and aragonite from sea water. *Geochimica et Cosmochimica Acta*, 39, 495-504.

Bischoff, W.D., Sharma, S.K. and Mackenzie, F.T. (1985) Carbonate ion disorder in synthetic and biogenic magnesian calcites: a Raman spectral study. *American Mineralogist*, 70, 581-589.

Bonales, L.J., Muñoz-Iglesias, V., Santamaría-Pérez, D., Caceres, M., Fernandez-Remolar, D. and Prieto-Ballesteros, O. (2013) Quantitative Raman spectroscopy as a tool to study the kinetics and formation mechanism of carbonates. *Spectrochimica Acta Part A*, 116, 26-30.

Canterford, J.H., Tsambourakis, G. and Lambert, B. (1984) Some observations on the properties of dypingite $Mg_5(CO_3)_4(OH)_2.5H_2O$. *Mineralogical Magazine*, 48, 437-442.

Chen, T., Neville, A. and Yuan, M.D. (2006) Influence of Mg^{2+} on $CaCO_3$ formation-bulk precipitation and surface deposition. *Chemical Engineering Science*, 61, 5318-5327.

Cipolli, F., Gambardella, B., Marini, L., Ottonello, G. and Vetuschi Zuccolini, M. (2004) Geochemistry of high-pH waters from serpentinites of the Gruppo di Voltri (Genova, Italy) and reaction path modelling of CO_2 sequestration in serpentinite aquifers. *Applied Geochemistry*, 19, 787–802.

Davies, P.J. and Bubela, B. (1973) The transformation of nesquehonite into hydromagnesite. *Chemical Geology*, 12, 289-300.

De Vito, C., Ferrini, V., Mignardi, S., Cagnetti, M. and Leccese, F. (2012) Progress in carbon dioxide sequestration via carbonation of aqueous saline wastes. *Periodico di Mineralogia*, 81, 333-344.

Dell, R.M. and Weller, S.W. (1959) The thermal decomposition of nesquehonite $MgCO_3 \cdot 3H_2O$ and magnesium ammonium carbonate $MgCO_3 \cdot (NH_4)_2CO_3 \cdot 4H_2O$. *Transactions of the Faraday Society*, 55, 2203-2220.

Edwards, H.G.M., Jorge Villar, S.E., Jehlicka, J. and Munshi, T. (2005) FT-Raman spectroscopic study of calcium-rich and magnesium-rich carbonate minerals. *Spectrochimica Acta Part A*, 61, 2273-2280.

Fernandez-Diaz, L., Putnis, A., Prieto, M. and Putnis, C.V. (1996) The role of magnesium in the crystallization of calcite and aragonite in a porous medium. *Journal of Sedimentary Research,* 66, 482-491.

Ferrini, V., De Vito, C. and Mignardi, S. (2009) Synthesis of nesquehonite by reaction of gaseous CO_2 with Mg chloride solution: Its potential role in the sequestration of carbon dioxide. *Journal of Hazardous Materials*, 168, 832–837.

Frost, R.L., Erickson, K.L. and Kloprogge, T.J. (2005) Vibrational spectroscopic study of the nitrate containing hydrotalcite mbobomkulite. *Spectrochimica Acta Part A*, 61, 2919-2925.

Frost, R.L. and Musumeci, A.W. (2006) Nitrate absorption through hydrotalcite reformation. *Journal of Colloid and Interface Science*, 302, 203-206.

Frost, R.L., Bahfenne, S. and Graham, J. (2009) Raman spectroscopic study of the magnesium carbonate minerals – artinite and dypingite. *Journal of Raman Spectroscopy,* 40, 855-860.

Goldsmith, J.R. (1953) A "simplexity principle" and its relation to "ease" of crystallization. *Journal of Geology,* 61, 439-451.

Hales, M.C., Frost, R.L. and Martens, W.N. (2008) Thermo-Raman spectroscopy of synthetic nesquehonite – implications for the geosequestration of greenhouse gases. *Journal of Raman Spectroscopy,* 39, 1141-1149.

Hopkinson, L.J., Rutt, K.J. and Cressey, G. (2008) The transformation of nesquehonite to hydromagnesite in the system $CaO-MgO-H_2O-CO_2$: an experimental spectroscopic study. *Journal of Geology*, 116, 387-400.

Hopkinson, L., Kristova, P., Rutt, K. and Cressey, G. (2012) Phase transitions in the system $MgO-CO_2-H_2O$ during CO_2 degassing of Mg-bearing solutions. *Geochimica et Cosmochimica Acta*, 76, 1-13.

Hu, Z. and Deng, Y. (2004) Synthesis of needle-like aragonite from calcite chloride and sparingly soluble magnesium carbonate. *Powder Technology*, 140, 10-16.

Hu, Z., Shao, M., Cai, Q., Ding, S., Zhong, C., Wei, X. and Deng, Y. (2009) Synthesis of needle-like aragonite from limestone in the presence of magnesium chloride. *Journal of Materials Processing Technology*, 209, 1607–1611.

Kamiya, K., Sakka, S. and Terada, K. (1977) Aragonite formation through precipitation of calcium carbonate monohydrate. *Materials Research Bulletin*, 12, 1095-1102.

Kazakov, A.V., Tikhomirova, M.M. and Plotnikova, V.I. (1959) The system of carbonate equilibria. *International Geological Review,* 1, 1-39.

Königsberger, E., Königsberger, L.-C. and Gamsjäger, H. (1999) Low temperature thermodynamic model for the system: Na_2CO_3-$MgCO_3$-$CaCO_3$–H_2O. *Geochimica et Cosmochimica Acta*, 63, 3105–3119.

Kristova, P., Hopkinson, L., Rutt, K., Hunter, H. and Cressey, G. (2013) Quantitative analyses of powdered multi-minerallic carbonate aggregates using a portable Raman spectrometer. *American Mineralogist,* 98, 401-409.

Loste, E., Wilson, R.M., Seshadri, R. and Meldrum, F.C. (2003) The role of magnesium in stabilising amorphous calcium carbonate and controlling calcite morphologies. *Journal of Crystal Growth*, 254, 206-218.

Martínez-Arkarazo, I., Angulo, M., Zuloaga, O., Usobiaga, A. and Madariaga, J.M. (2007) Spectroscopic characterisation of moonmilk deposits in Pozalagua tourist Cave (Karrantza, Basque Country, North of Spain). *Spectrochimica Acta Part A*, 68, 1058-1064.

Menzel, H. and Brückner, A. (1930) Studien an kohlensauren Magnesiumsalzen. I. Basische Magnesiumcarbonate. *Zeitschrift für Elektrochemie und angewandte physikalische Chemie,* 36**,** 63–87.

Mignardi, S., De Vito, C., Ferrini, V. and Martin, R.F. (2011) The efficiency of CO_2 sequestration via carbonate mineralization with simulated waste waters of high salinity. *Journal of Hazardous Materials,* 191, 49-55.

Morse, J.W. and Casey, W.H. (1988) Ostwald processes and mineral paragenesis in sediments. *American Journal of Science*, 288, 537-560.

Munemoto, T. and Fukushi, K. (2008) Transformation kinetics of monohydrocalcite to aragonite in aqueous solutions. *Journal of Mineralogical and Petrological Sciences,* 103, 345-349.

Nishiyama, R., Munemoto, T. and Fukushi, K. (2013) Formation condition of monohydrocalcite from $CaCl_2$–$MgCl_2$–Na_2CO_3 solutions. *Geochimica et Cosmochimica Acta*, 100, 217-231.

Orlando, A., Lelli, M. and Marini, L. (2012) Production of amorphous hydrated impure magnesium carbonate through *ex situ* carbonation. *Applied Geochemistry*, 27, 2500–2510.

Park, W.K., Ko, S.-J., Lee, S.W., Cho, K.-H., Ahn, J.-W. and Han, C. (2008) Effects of magnesium chloride and organic additives on the synthesis of aragonite precipitated calcium carbonate. *Journal of Crystal Growth*, 310, 2593–2601.

Queralt, I., Juliá, R., Plana, F. and Bischoff, J.L. (1997) A hydrous Ca-bearing magnesium carbonate from playa lake sediments, Salines Lake, Spain. *American Mineralogist,* 82, 812–819.

Reddy, M.M. and Wang, K.K. (1980) Crystallization of calcium carbonate in the presence of metal ions. *Journal of Crystal Growth*, 50, 470-480.

RRUFF database - Chlorartinite (ID no. R060878), available at http://rruff.info/chlorartinite, (Accessed: 12th February 2014).

Taylor, G.F. (1975) The occurrence of monohydrocalcite in two small lakes in the south-east of South Australia. *American Mineralogist*, 60, 690-697.

White, W.B. (1974) The carbonate minerals, in: Farmer, V.C. (Ed.) *The infrared spectra of minerals*, Mineralogical Society, London, Monograph 4, Chapter 12, 227-284.

Zhang, Z., Zheng, Y., Ni, Y., Liu, Z., Chen, J. and Liang, X. (2006) Temperature and pH dependent morphology and FT-IR analysis of magnesium carbonate hydrates. *Journal of Physical Chemistry B*, 110, 12969-12973.